Overview of the Initial NSTX Experimental Results

M. ONO 1), M. BELL 1), R. E. BELL 1), T. BIGELOW 2), M. BITTER 1), W. BLANCHARD 1), D. DARROW 1), E. FREDRICKSON 1), D. GATES 1), L. GRISHAM 1), J. HOSEA 1), S. M. KAYE 1), R. KAITA 1), S. KUBOTA 9), H. KUGEL 1), D. JOHNSON 1), B. LEBLANC 1), R. MAINGI 2), R. MAQUEDA 5), E. MAZZUCATO 1), J. MENARD 1), D. MUELLER 1), B. A. NELSON 4), C. NEUMEYER 1), F. PAOLETTI 3), S. PAUL 1), Y-K.M. PENG 2), S. RAMAKRISHNAN 1), R. RAMAN 4), P. RYAN 2), S. SABBAGH 3), C. SKINNER 1), T. STEVENSON 1), D. STUTMAN 7), E. SYNAKOWSKI 1), D. SWAIN 2), G. TAYLOR 1), A. VON HALLE 1), J. WILGEN 2), M. WILLIAMS 1), J.R. WILSON 1),), S. ZWEBEN 1), R. ACKERS 19), R.E. BARRY 2), A. BERS 12), J. BIALEK 3), P. BONOLI 12), M. D. CARTER 2), J. CHRZANOWSKI 1), W. DAVIS 1), E. DOYLE 9), L. DUDEK 1), R. ELLIS 1), P. EFTHIMION 1), J. FERRON 6), E. FREDD 1), M. FINKENTHAL 7), T. GIBNEY 1), R. GOLDSTON 1), R. E. HATCHER 1), R. HAWRYLUCK 1), H. HAYASHIYA 14), K. HILL 1), T. JARBOE 4), S. C. JARDIN 1), H. JI 1), M. KALISH 1), L. LAO 6), K.C. LEE 11), F. LEVINTON 14), N.C. LUHMANN 11), P. LAMARCHE 1), B. MCCORMACK 1), R. MAJESKI 1), J. MANICKAM 1), R. MARSALA 1), T. K. MAU 10), S. MEDLEY 1), M. M. MENON 2),O. MITARAI 17), M. NAGATA 18), N. NISHINO 16), G. OLIARO 1), H. PARK 1), R. PARSELLS 1), T. PEEBLES 9), G. PEARSON 1), C.K. PHILLIPS 1), R. PINSKER 6), G.D. PORTER 13), A.K. RAM 12), J. ROBINSON 1), P. RONEY 1), L. ROQUEMORE 1), A. ROSENBERG 1), M. SCHAFFER 6), S. SHIRAIWA 15), P. SICHTA 1), B. STRATTON1), D. STOTLER 1), Y. TAKASE 15), W. R. WAMPLER 8), G. WURDEN 5), J. G. YANG 20), X. Q. XU 13). L. ZENG 9), W. ZHU 3)

1) Princeton Plasma Physics Laboratory, Princeton, NJ, USA
2) Oak Ridge National Laboratory, Oak Ridge, TN, USA,
3) Columbia University, New York, NY, USA
4) University of Washington, Seattle, WA, USA
5) Los Alamos National Laboratory, Los Alamos, NM, USA
6) General Atomics, San Diego, CA, USA
7) Johns Hopkins University, Baltimore, MD, USA
8) Sandia National Laboratory, Albuquerque, New Mexico, USA
9) UC Los Angeles, Los Angeles, CA, USA
10) UC San Diego, San Diego, CA, USA
11) UC Davis, Davis, CA, USA
12) Massachusetts Institute of Technology, Cambridge, MA, USA
13) Lawrence Livermore National Laboratory, Livermore, CA, USA
14) Fusion Physics, and Technology, San Diego, CA, USA
15) Univ. Tokyo, Tokyo, Japan
16) Hiroshima Univ., Hiroshima, Japan
17) Kyushu Tokai Univ., Kumamoto, Japan
18) Himeji Inst. Technology, Okayama, Japan
19) EURATOM/UKAEA. Culham, UK
20) Korea Basic Science Institute, Taejeon, Korea

e-mail contact of main author: mono@pppl.gov

Abstract. The main aim of National Spherical Torus Experiment (NSTX) is to establish the fusion physics principles of the spherical torus (ST) concept. The NSTX device began plasma operations in February 1999 and the plasma current I_p was successfully brought up to the design value of 1 million amperes on December 14, 1999. The planned plasma shaping parameters, elongation κ = 1.6 – 2.2 and triangularity δ = 0.2 – 0.4, were achieved in inner limited, and single-null and double-null divertor configurations. The CHI (Coaxial Helicity Injection) and HHFW (High Harmonic Fast Wave) experiments were also initiated. CHI injected current of 27 kA produced up to 260 kA

toroidal current without using an ohmic solenoid. With injection of 2.3 MW of HHFW power, using twelve antennas connected to six transmitters, electrons were heated from a central temperature of 400 eV to 900 eV at a central density of 3.5 x 10^{13} cm^{-3} increasing the plasma energy to 59 kJ and the toroidal beta, β_T to 10 %. The NBI system commenced operation in Sept. 2000. The initial results with two ion sources (P_{NBI} = 2.8 MW) shows good heating producing a total plasma stored energy of 90 kJ corresponding to $\beta_T \approx 18$ % at a plasma current of 1.1 MA.

1. Motivation and mission of NSTX

A broad range of encouraging advances has been made in the exploration of the Spherical Torus (ST), a very low aspect-ratio tokamak concept [1]. A schematic of the ST magnetic configuration is shown in Fig. 1. These advances include promising experimental data from pioneering experiments [2-4], theoretical predictions [5,6], near-term fusion energy development projections such as the Volume Neutron Source [7], and future applications to power plants [8]. The National Spherical Torus Experiment (NSTX) is a U.S. national research facility located at Princeton Plasma Physics Laboratory (PPPL) focused on ST related research with an emphasis on finding a cost-effective route to an attractive fusion power plant. Its main mission is to extend the understanding of toroidal plasma physics to new regimes at the mega-ampere level at high plasma beta [9,10]. The key physics objective of NSTX is to attain an advanced ST regime; i.e., simultaneous ultra high beta (β), high confinement, and high bootstrap current fraction (f_{bs})[6]. This regime is considered essential for the development of an economical power plant because it minimizes the recirculating power and power plant core size. Other NSTX mission elements crucial for ST power plant development are the demonstration of fully non-inductive operation and the development of acceptable power and particle handling concepts.

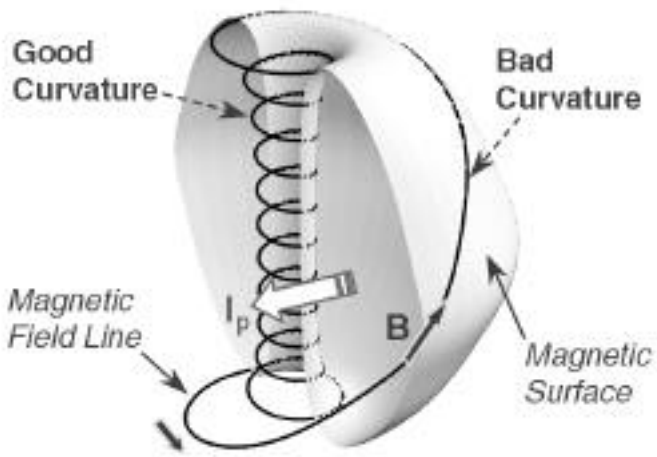

Fig. 1. The ST Configuration maximizes the field line length in the region of favorable curvature.

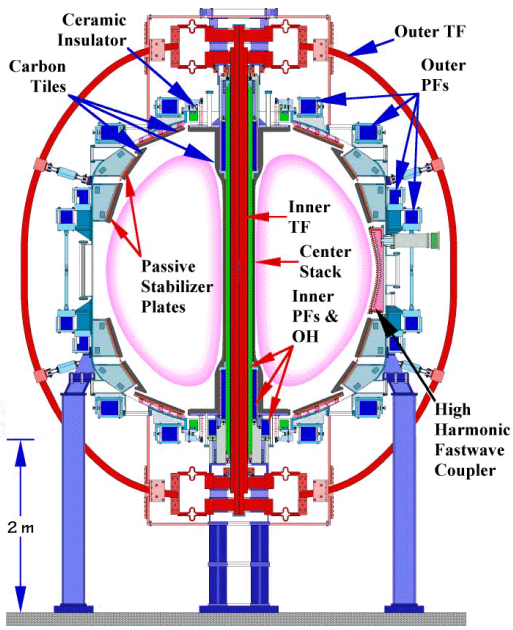

Fig. 2. NSTX Device Cross Section

2. NSTX Facility Design Capability and Technology Challenges

The NSTX facility [11] is designed to achieve the NSTX mission with the following capabilities:

- Aspect ratio R/a ≥ 1.26, including a 0.6 Weber OH solenoid and coaxial helicity injection (CHI)[4,12] for plasma startup
- I_p = 1 MA for low collisionality at relevant densities
- High Harmonic Fast Wave [13] (HHFW - 6 MW, 5 s), Coaxial Helicity Injection (CHI – $I_{inj} \leq$ 50 kA at 1 kV), Neutral Beam Injection (NBI - 5 MW, 5 s) for heating and j(r) control
- Close-fitting conducting shell for maximum β_T and Troyon-normalized beta value β_N
- Pulse length 5 s ≥ skin time ≈ L/R time

The NSTX device is schematically shown in Fig. 2. The coil system configuration allows strong plasma shaping, e.g. $I_p q_{95} / aB$, can reach as high as 60, an order of magnitude greater than that achieved in conventional aspect-ratio tokamaks. The demountable center stack [composed of the inner toroidal field (TF) coil bundle, the Ohmic heating (OH) solenoid, the inner poloidal field (PF) coils, the thermal insulation, the Inconel vacuum casing, and the graphite plasma facing components with over 200 sensor elements] is the most critical component of NSTX [14]. The center stack is isolated from the outer vessel by ceramic insulators and bellows to provide electrical isolation for CHI and mechanical isolation to allow for the thermal expansion of the center-stack with respect to the outer vacuum vessel during bakeout and operations. The demountable center stack facilitates the construction, maintenance and/or future upgrading of the device. The NSTX device is equipped with closely-fitting 1.2 cm thick copper passive stabilizing plates for MHD mode stabilization. CHI and HHFW will be used for the initial plasma start-up studies. An innovative design was developed for the 12 element HHFW antenna decoupler / matching system powered by 6 RF transmitters providing total power of 6 MW up to 5 s. One of the TFTR NBI systems (with three ion sources) is installed to inject total power of 5 MW at 80 kV for up to 5 s. Indeed, the NSTX facility utilizes much of the former TFTR facility at PPPL. After three years of design and construction, NSTX became operational in Feb. 1999.

3. Progress on Ohmic Operations

3.1 First Plasma and Achievement of 1 MA Plasma Current Discharges - On Feb. 12 1999, a fast camera observed the first “flash” of ohmic plasma, which reached about 20 kA of plasma current. Within the following two days of plasma operations, the plasma current reached the 300 kA level, which is close to the predicted value for the OH flux used (about 1/3 of the design flux.) The device capability was increased relatively quickly, and on Dec. 16, 1999 the plasma current was raised to the device design value of 1MA. Key to the achievement of high current plasma discharges was the implementation of the real time plasma control system which controls the plasma radial and vertical positions as well as the plasma current [15].

An electron cyclotron heating preionization (ECH-P) system proved to be helpful in plasma initiation. The 18 GHz unit is capable of delivering 30 kW of ECH-P power for 100 ms. The ECH-P creates a vertically uniform plasma sheet at the electron cyclotron resonant layer which is at R = 42 cm for the nominal 3 kG toroidal field at the vacuum vessel center R = 85 cm. The ECH-P makes the OH plasma initiation less sensitive to error fields, enhancing the operational flexibility. Another utilization of ECH-P is for the low gas pressure start-up of the Coaxial Helicity Injection (CHI). It is important for CHI to be able to operate in a sufficiently low neutral pressure range to be compatible with the ohmic operations. The ECH-P helps breakdown even at low neutral fill pressure, aiding the CHI start-up.

3.2 Ohmic Plasma Equilibrium - In Fig. 3, a comparison of visible light emission from the plasma imaged at 1 kHz [16] and the plasma configuration calculated by the EFIT code based on external magnetic data with 1 ms resolution [17] are shown. The three frames are an early small-bore plasma, the transition to a lower single null diverted plasma, and the return to the center stack limited plasma, respectively. These features are all consistent with the details of the reconstructed plasma boundary shape.

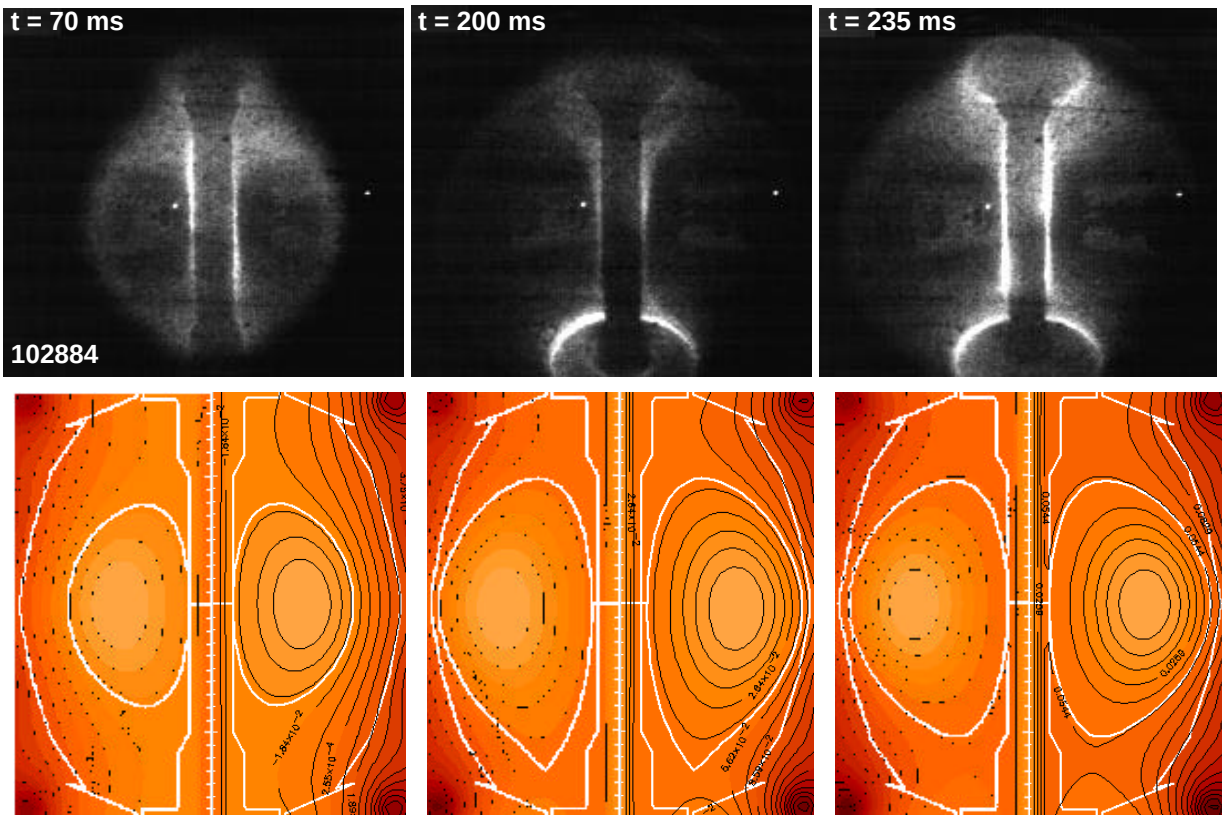

Fig. 3. Comparison of visible-light images of the evolution of the plasma boundary and EFIT magnetic reconstructions. The discharge time is as shown.

The evolution of this 700 kA level plasma is shown in Fig. 4. The plasma transiently reached an elongation of 2.5 and triangularity of 0.6, with nominal flattop values of 2.0 and 0.4 respectively. Plasma internal inductance generally increases from 0.3 to ~ 1.0 during a discharge. A plasma shaping factor (I_p q_{95} / a B) of 30 has been thus far achieved at 1 MA. Ohmic plasmas with volume in excess of 12 m^3 have been routinely produced. The plasma configurations of inner wall limited, single null and double null diverted discharges were successfully created. Each configuration has been produced with a nominally constant plasma current for durations of 3 - 5 energy confinement times. The plasma shaping parameters accessed in the ohmic discharges are shown in Fig. 4 where the achieved elongation κ and triangularity δ are plotted. These elongations and triangularities span much of the range of operating space expected from model calculations.

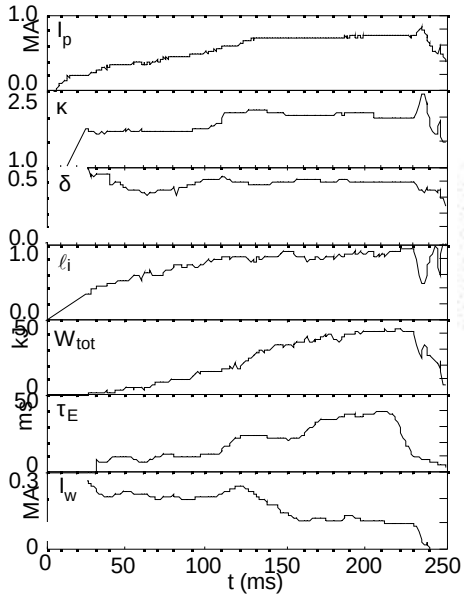

Fig. 4.: A typical plasma discharge Evolution.

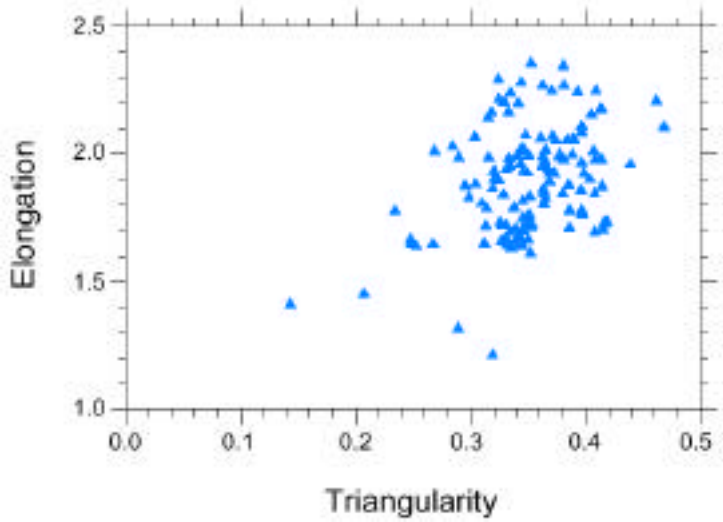

Fig. 5. Achieved plasma shaping parameters.

3.3 Ohmic Flux Consumption and Boronization – In order to optimize the ohmic flux consumption, various plasma current ramp-up rates have been investigated [18]. By convention, the resistive flux consumption is parameterized with the Ejima coefficient C_E and the total surface flux consumption is parameterized here using the Ejima-Wesley coefficient $C_{E\text{-}W}$ [18, 19]. Application of a boron coating on the plasma facing components using a glow discharge in a mixture of deuterized trimethylboron (TMB) and helium has significantly reduced the metallic and oxygen impurity level in NSTX plasmas. In Fig. 6, comparison shots before and after boronization are shown. The boronization not only reduced the loop-voltage and ohmic flux consumption, thus extending the pulse length, but it also reduced the MHD activity (Fig. 4). Figure 7 plots Ejima coefficients and the internal inductance for discharges of varied ramp-rates, both pre- (dashed) and post-boronization (solid) in deuterium with line-average densities of 2-4 × 10^{13} cm^{-3} at peak current. The figure shows, as expected, that faster ramps reduce flux consumption by reducing both the resistive dissipation (a) and internal inductance (b). In practice, average ramp- rates of 5-6 MA/s are routinely used, while faster ramps become increasingly prone to MHD events. The total flux consumption during the ramp-up phase also dropped by 20% after boronization as shown in Fig. 7. Most of the decrease comes from a decrease in the internal inductance at fixed ramp-rate**.** We should note here that an important role is played by MHD activity (which is described in more detail in Sec. 3.5) on the ohmic flux consumption and the flat-top time. If a major MHD event (such as the one occurring at 0.2 sec for pre-boronization shot and at 0.26 sec for the post-boronization shot as shown in Fig. 6), the core plasma temperature cools rapidly, essentially ending the flat top since the OH voltage available at the end of the pulse is not sufficient to maintain the current. If the OH flux and loop voltage are available, it is possible to recover from such MHD events as shown for the pre-boronization shot at t = 140 msec in Fig. 6. Therefore in addition to the impurity control in order to optimize the flux consumption and maximize the flat top pulse duration, it is also important to keep the major MHD instabilities from occurring.

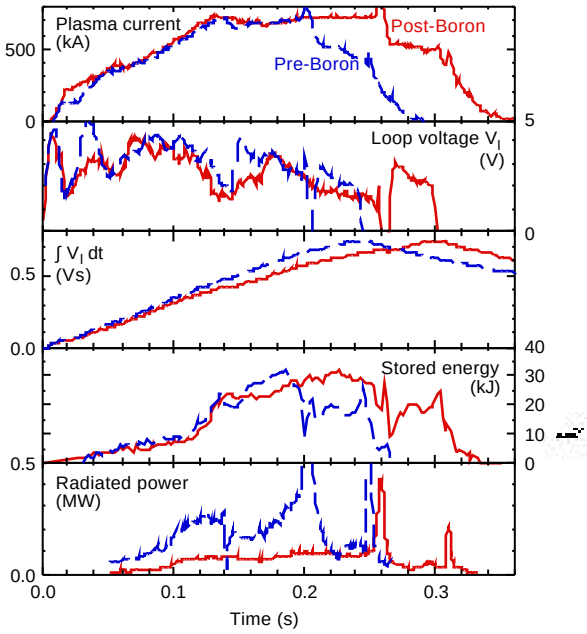

Fig. 6. Effect of boronization on the Ohmic discharges.

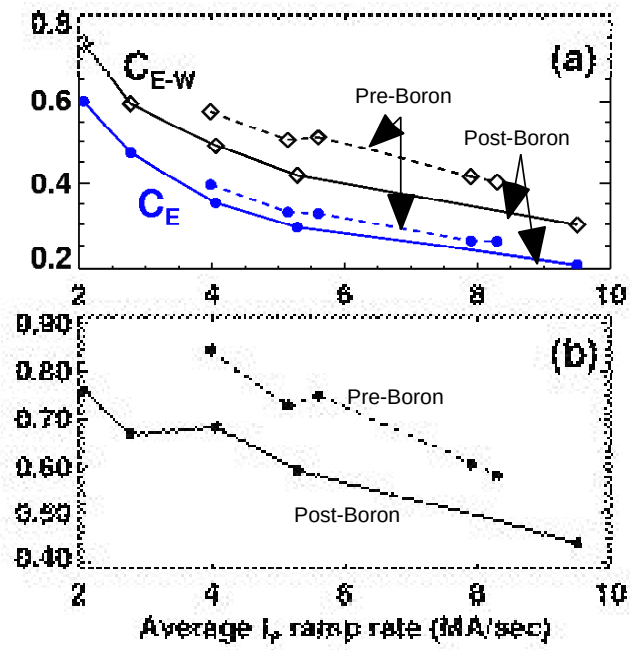

Fig. 7. (a) Ejima and Ejima-Wesley coefficient vs. ramp-rate. (b) Internal inductance vs. ramp-rate

3.4 Density Limits and Global Energy Confinement – The density limits and global energy confinement were investigated for the plasma current range of 600 – 900 kA. The density limits observed in NSTX generally improved over the time as the plasma conditions improved through wall conditioning. In particular, the TMB boronization improved the density operating range significantly as shown in Fig. 8. The effect of the boronization was to increase the achievable densities in both species. Densities (line averaged) greater than 4×10^{19} m^{-3} were attained only in post-boronized helium plasmas. As shown in Fig. 9, the deuterium density limit increased from approximately 60 % of the Greenwald limit density ($n_{eGW} \equiv I_p/\pi a^2$) for the pre-boronization level to about 75 to 80% of the limit, while the helium density limit increased from about 75% of the limit (pre-boronization) to the Greenwald limit and even a bit beyond. At present, our observation seems to point to a "soft" density limit**.** There is no obvious event such as radiation collapse, marfe, sawtooth, etc. correlated with the limit. This is probably due to the fact that the radiated power fraction is still small (≤ 30%) even at the highest density. Also, there is no obvious global MHD modes coming in at high density. We therefore believe that the present maximum density is due to our limited gas-puff (fueling) capability.

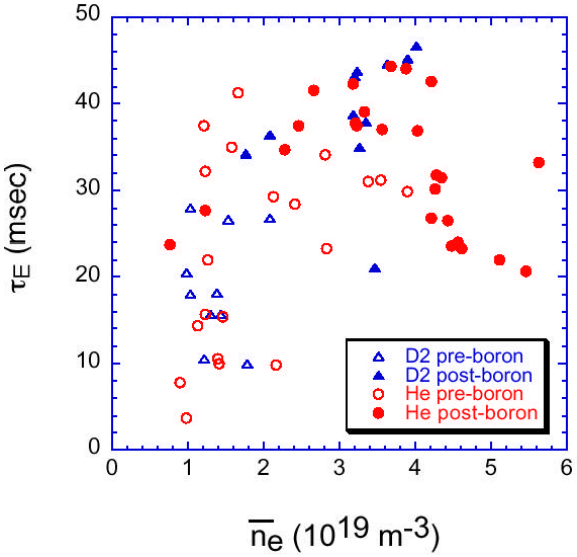

Fig. 8. Energy confinement time vs. plasma density. Ip = 600 – 900 kA

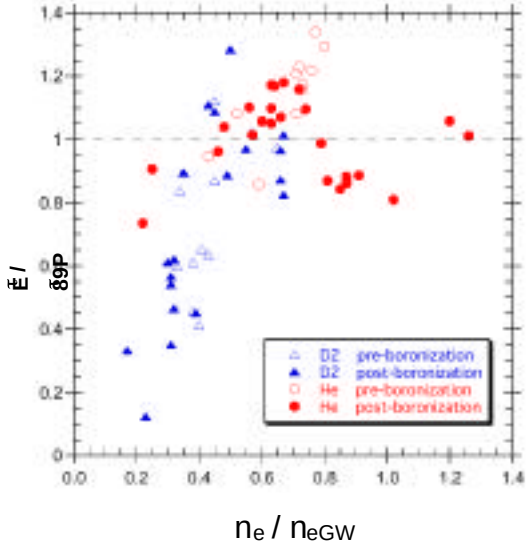

Fig. 9. ITER 89P normalized energy confinement time vs. Greenwald normalized plasma density.

Confinement times in both deuterium and helium ohmic plasmas exhibit trends that are similar to those at conventional aspect ratio and they are summarized in Figs. 8 and 9. For low to moderate densities ($\leq 4\times10^{13}$ cm^{-3}, corresponding to $n_e/n_{eGW} \leq 0.8$), the confinement time in both species increases approximately linearly with line-averaged density to a value of 45 ms. At $n_e/n_{eGW} \leq 0.8$, the maximum confinement time is approximately 1.4 $\tau_{ITER89P}$, [20] while $\tau_E/\tau_{ITER89P}$ = 0.8-1.0 at the higher densities. The confinement time drops to values of about 20 ms at the highest density (5.5×10^{19} m^{-3}), corresponding to $n_e/n_{eGW} \approx 1.2$. For the ITER89P scaling in used in Fig. 9, the mass scaling parameter was taken to be M_{eff}/Z_{ion}, which is 2 for either species. This is consistent with the observed similar confinement behavior for helium and deuterium discharges. One major difference between the deuterium and helium higher density discharges was the amount of carbon influx as indicated by the CIII light, which was much greater in deuterium plasmas presumably due to chemical sputtering of the graphite tiles. For both species, in both the pre- and post-boronized plasmas, the radiated power was typically ≤ 30% of the ohmic heating power at the time of maximum density.

3.5 MHD Activity – A variety of MHD activity including reconnection events and sawtooth activity is observed in NSTX. The reconnection events depend particularly strongly on the wall conditions. During the first plasma operations with the newly fabricated vacuum vessel and partial graphite-tile wall coverage, MHD activity was observed throughout the discharge. As the discharge conditions improved, the frequency of the MHD events decreased. The complete graphite tile coverage together with wall conditioning (baking, glow discharge cleaning and boronization) helped to reduce the frequency of the MHD events. MHD events now occur particularly during the current ramp down phase. With an appropriate gas-puff, it is possible to ramp down without the events for some discharges. Presently, the dominant MHD mode appears to be the toroidal mode number n = 1 mode, though some higher n number and higher frequency modes have been observed. In Fig. 10(a), the plasma evolution illustrating the

deleterious effect of a sawtooth is shown. A significant core pressure reduction occurs when the sawtooth activity starts. From the EFIT magnetic reconstruction, the start of sawtooth

activity coincides well with the appearance of the $q_0 = 1$ surface as showing Fig 10(b). Due to the strong shaping and toroidicity (low-aspect-ratio) of NSTX, the EFIT reconstruction contains significant internal profile information, such as the pressure and q-profiles. The agreement between the soft x-ray sawtooth inversion layer and q = 1 surface is surprisingly good. As can be seen from the Fig, 10(b), due to the large radius position of the q = 1 layer, the sawtooth crash in NSTX causes significant degradation to the plasma performance by causing the central pressure to collapse. It is therefore quite clear that we must control the plasma current profile so that the q_0 stays well above 1.

3.6 Plasma Disruptions and Wall Halo Currents – The plasma disruption (i.e. rapid plasma current termination event) and generation of wall halo currents remain critical issues for tokamak reactor designs due to the high stress on the wall and PFCs imparted by the $j_{pol} \times B_T$ force of the halo-induced wall currents. In the CDX-U and START devices, the plasma halo currents have been measured to be only a small fraction, below 5%, of the peak plasma current [2,3]. Recent MAST results also support this rather benign trend for the ST [21]. On NSTX, halo currents have been measured in the center column as well as in the passive stabilizer plate support legs. While plasma disruptions (very rapid current terminations) can be avoided most of the time, it is prudent to design a fusion reactor to withstand disruptions. On NSTX, disruptions are indeed observed. The fastest plasma current decays were observed during the so-called VDE (Vertical Displacement Event) due to the loss of vertical stability (ideal MHD equilibrium. In Fig. 11(a), a plasma disruption with the plasma current ramp-down rate of 400 MA/s (the fastest thus far observed) is shown.). This example occurred during the experiments to test the vertical stability limits and feed-back control system. Figure 11(b) shows that the induced CS casing current (solid line) measured by a Rogowski coil located near the end of the center-stack has a peak magnitude of 20-30kA. This corresponds to 3-5% of the maximum plasma current. Figure 11(b) also shows the toroidal current induced on the outboard lower primary passive plate peaks at approximately 10kA. These halo-induced wall currents are therefore relatively modest and benign from the device design point of view. We should note that this type of fast current decay is quite rare, usually not present in the normal NSTX discharges. Instead, the plasma current of typical discharges ramps down with a series of MHD events over tens of msec as shown in Fig. 10a. We see very little halo-induced current for this case.

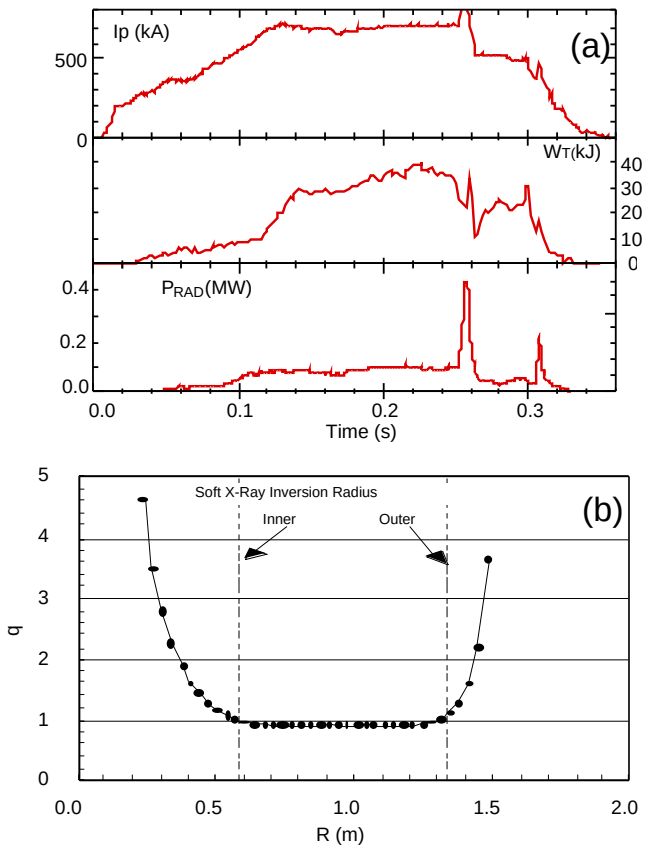

Fig. 10. MHD Behavior. (a) Ohmic discharge with a sawtooth crash. (b) EFIT q profile versus major radius and position of soft x-ray inversion radius.

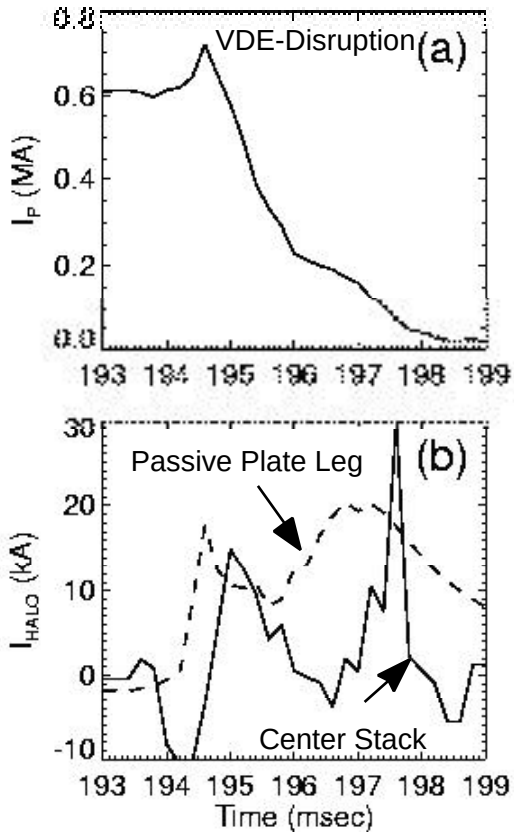

Fig. 11. Disruption and halo- evolution with induced currents. (a) Plasma current decay during disruption. (b) Wall-induced currents in the center stack (solid curve) and the passive plate leg (dashed curve).

4. Co-axial Helicity Injection Plasma Start-up

For an attractive ST power plant, the OH solenoid must be eliminated in the center stack. The relatively modest magnetic flux and helicity per unit plasma current for the ST tend to ease noninductive startup requirements. The main tool being tested for NSTX is the coaxial-helicity-injection (CHI). The concept has been investigated previously in smaller experimental devices including HIT/HIT-II [4] and HIST [12]. An experimental set-up of CHI is shown in Fig. 12. Because of the ceramic insulating rings located at the top and bottom of the device, the center-stack is electrically insulated from the outer vacuum vessel, allowing bias voltage to be applied. With appropriate gas fill pressure (typically in a few m-Torr range) and with a voltage of up to 1 kV applied, a plasma discharge is initiated. Using appropriate poloidal field coils (as shown in Fig. 12), stronger poloidal fields are applied near the bottom gap, to reduce the connection length, so that the discharge is initiated preferentially in the lower gap region. The applied toroidal field causes the current in the plasma to develop a strong toroidal component, the beginning of the desired toroidal plasma current. If the injector current exceeds a threshold

value, the resulting ΔB_{tor}^2 or ($\mathbf{J}_{pol}$ x $\mathbf{B}_{tor}$) stress across the current layer exceeds the field line tension of the injector flux causing the helicity and plasma in the lower divertor region to move into the main torus chamber. It should be noted that the CHI system capability on NSTX is a significant extension of the previous CHI experiments in that the plasma volume and pulse length are increased by a factor of about 30 [22]. In Fig. 13, typical CHI discharge waveforms are shown in which the toroidal current is driven from zero current without the ohmic solenoid. The discharge has 200 ms pulse length with a flat top toroidal current of 200 kA. To date, CHI in NSTX has driven toroidal plasma current of up to about 260 kA transiently with injection of about 27 kA, yielding current amplification factor of ≈ 10. Our near term goal is to drive ≈ 500 kA toroidal current with 50 kA injection current. The CHI capability thus developed on NSTX will be used to assist the current ramp-up to about 1 MA and to provide edge current drive for current profile control. If the CHI plasma can be formed with about $T_e \approx 200$ eV, then it would be possible to heat and drive current in the start-up phase of the plasma by HHFW. This would go a long way to realize fully non-inductive current start-up for ST.

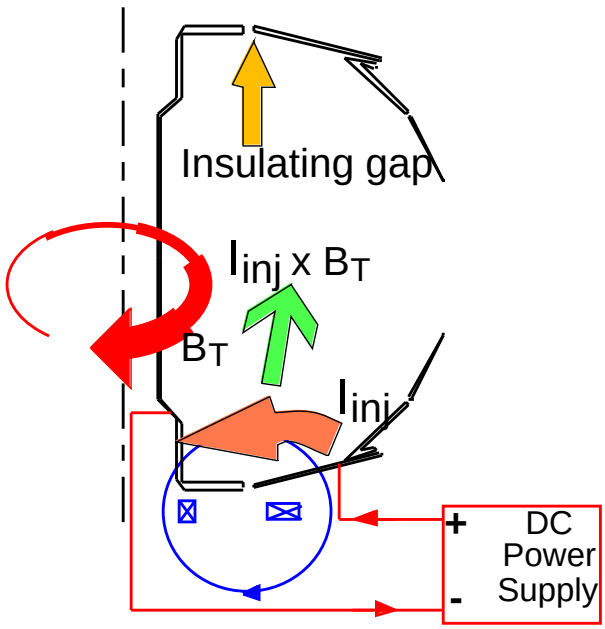

Fig. 12. Schematic of CHI Experimental setup.

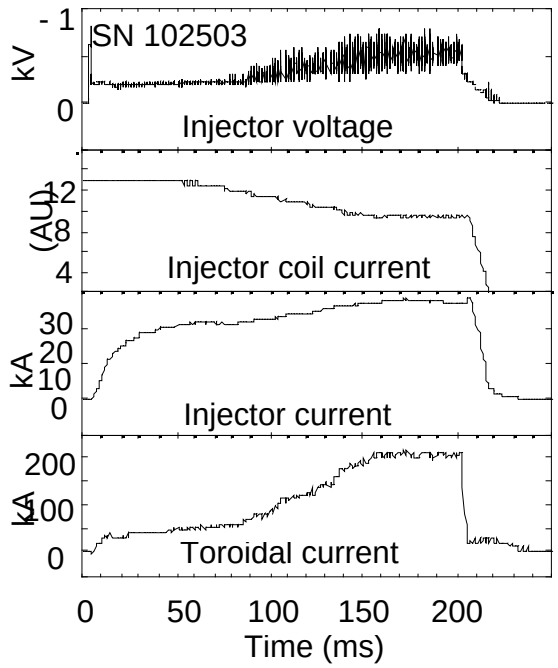

Fig. 13 CHI discharge evoluation.

5. High Harmonic Fast Wave Heating

High harmonic fast wave (HHFW) research is appropriate for NSTX due to the high beta and high plasma dielectric constant, $\varepsilon \equiv (\omega_{pe}/\Omega_e)^2$. For example, the NSTX plasmas typically operate in $\varepsilon = 10 - 100$ range compared to the typical tokamak experiment of $\varepsilon \leq 1$. The central plasma toroidal beta in NSTX is well above 10% and is expected to reach the 50 – 100% ranges. This requirement is similar to that in other compact confinement devices such as the Spheromaks, RFPs, and FRCs. In this regime, the conventional electron heating and current drive tools such as Electron Cyclotron Heating and Lower Hybrid Current Drive cannot be used due to the lack of wave accessibility. The HHFW is predicted to be able to access high dielectric plasmas and heat electrons efficiently via transit time magnetic pumping and electron Landau damping [8]. The NSTX antenna phasing system is capable of varying the parallel wave number $k_{\parallel}$ from 14 m^{-1} to about 4 m^{-1} in real time in order to follow the plasma discharge evolution from

low temperature (≈ 300 eV) start-up plasmas to high temperature (few keV) high beta plasmas in real time [24].

The HHFW electron heating experiments thus far have concentrated on efficient coupling of power into the plasma with a known phase. Plasma currents from 500 to 700 kA in helium and deuterium have been explored. Center stack limited and double null diverted discharges were employed. The gap between the plasma boundary and the antenna shield was varied from essentially zero to 10 cm or more. A gap of around 5 cm was found to be optimal. Figure 14 shows the time evolution of a HHFW heated, 700 kA helium plasma discharge where 2.3 MW of HHFW power with the slowest phasing (i.e., $k_{\parallel} \approx 14\ m^{-1}$) is applied starting at 160 ms. In Fig. 15, the density and electron temperature profiles from Thomson scattering at t = 230 ms are shown. The central electron temperature increases from 400-500 eV to 900 eV during the rf heating while the central density remains constant. The temperature increase is broad in radius and accompanied by little density increase. This is

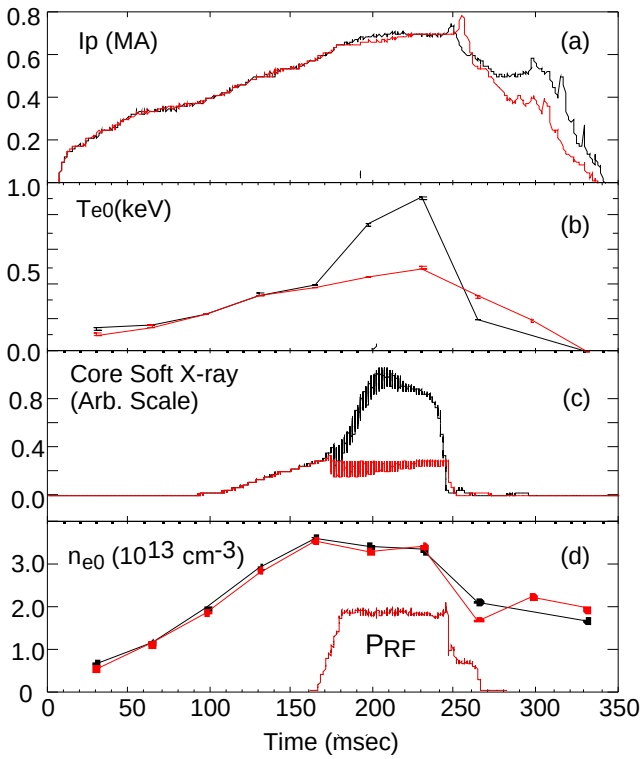

Fig. 14. Discharge evolution with and without RF. P_{rf} = 2.3 MW, $k_{\parallel} \approx 14\ m^{-1}$, B_T = 3 kG,

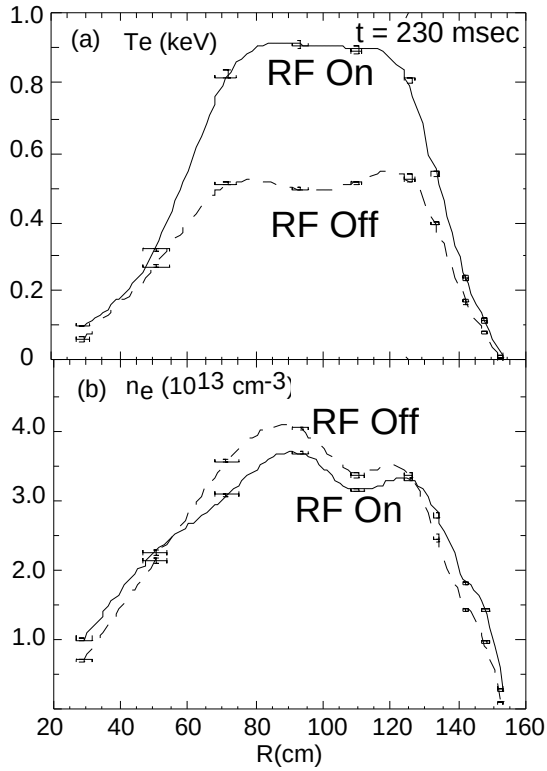

Fig. 15. Thomson scattering electron temperature and electron density. β_T = 10%, W_T = 60 kJ, ε = 40

consistent with the slow-phase-velocity wave heating, where the heating deposition is expected to broaden as the central electron temperature is increased [23]. The loop voltage falls to 1.0 V as compared to 1.35 V on an identical plasma without rf. Confirmation of the temperature increase is also seen with an x-ray crystal spectrometer, which yields a central temperature of about 1 keV. The central plasma density was relatively constant at about 3.5 x 10^{13} cm^{-3} corresponding to $\varepsilon \approx 40$. A maximum stored energy of 58 kJ and $\beta_T \equiv 2\ \mu_0 < p > / B_{T0}^2$ = 10% (where B_{T0} is the vacuum toroidal magnetic field at the geometric axis) with 2.9 MW of power was obtained. The HHFW electron heating has been observed with the ohmic plasmas with the electron temperature as low as 200 eV. Plasma radiation as measured by bolometry shows an increase in edge radiation, which is attributed to carbon. The total radiated power however remains very low at < 15. %

6. Initial Neutral Beam Heating Results

6.1 NBI Heating Dependence on Plasma Current and Ion Source - A neutral beam injector (5 MW – 80 keV) from TFTR was installed on NSTX, and the system was commissioned in Sept 2000. The initial NBI heating experiment was conducted with two ion sources with total power of up to 2.8 MW. The tangency radius of the two operating sources are Source B: R = 50 cm and Source C: R = 60 cm, which are "off-axis" heating sources compared to the plasma axis at R ≈ 90 cm, as shown in Fig. 16. At 80 keV, injected beam ions have larger prompt orbit loss for lower plasma current as well as for Source C (compared to Source B) located more off-axis. In Fig. 17, the observed stored energy increase for a given source power of 1.4 MW for Source B, C, and B + C combined for various plasma currents is shown. The stored energy increment increases with the plasma current as expected. At 900 kA, the stored energy increment for two sources becomes comparable. As the current is decreased to 700 kA, the Source C shows a rapid decrease in heating efficiency, while Source B is still heating relatively well. At 500 kA, the heating efficiency for both sources drops dramatically, which is consistent with prompt orbit loss calculations [24].

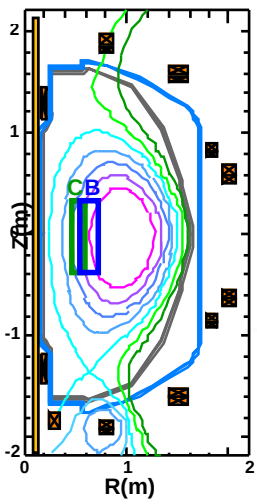

Fig. 16. NBI tangency foot prints for Sources B, and C.

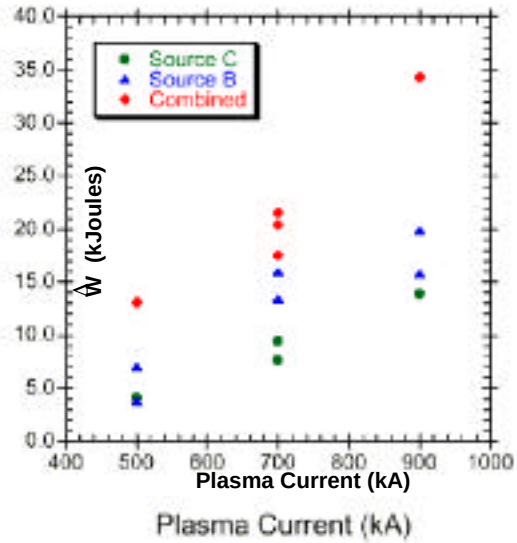

Fig. 17, Incremental Total Stored Energy vs. Plasma Current for ion sources B and C each Providing 1.4 MW.

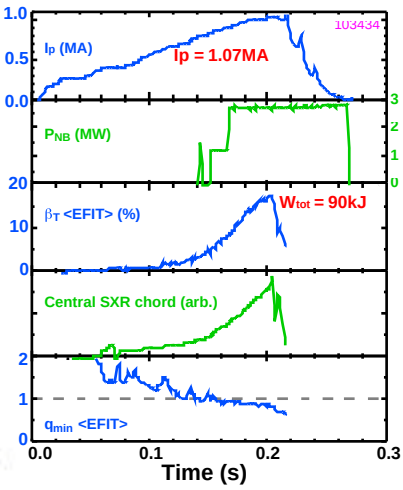

Fig. 18. Time evolution of NBI heated discharge: B_T = 3 kG, Deuterium.

6.2 High Beta Discharges – With outer two ion sources (B and C) operating at 80 keV, the initial NBI plasma heating was investigated with $P_{NBI} \approx 2.8$ MW. The discharge evolution for a high beta discharge is shown in Fig. 18. As seen in the figure, the plasma current approaches a record value for the ST of ≈ 1.1 MA peak current with B_T = 3 kG. The total plasma stored energy increases to our record value of β_T = 18% corresponding to 90 kJ of total plasma stored energy as measured through the EFIT reconstruction. The EFIT magnetic reconstruction values have a typical uncertainty of about 20% [17]. The Troyon normalized beta, $\beta_N \equiv 10^8\, \beta_T\, a\, B_T / Ip$ is about 3 for this discharge. The EFIT reconstructed plasma poloidal flux contour cross section is shown in Fig. 16. However, around t = 200 ms, the plasma beta collapses as shown in Fig. 18. The central temperature drops rapidly as can been seen with the central soft x-ray channel trace. We observe that prior to the beta collapse, the n=1/m=1 mode is growing and eventually triggers

a sawtooth instability, causing this beta collapse. This collapse mechanism is essentially the same as the one observed with ohmic plasmas, as discussed in the previous section. The collapse time correlates well with the central q q_0 going below one, as seen by EFIT. This sawtooth collapse should be avoidable by discharge evolution programming and non-inductive current drive to maintain q_0 above 1. The achievement of β_T of 18 % with a relatively small injected power of 2.8 MW is a very encouraging indication of the effectiveness of NBI in obtaining high beta discharges in NSTX.

7. Summary and Future Plans

The NSTX facility commenced operation in Feb. 1999. The plasma current was successfully brought up to the design value of 1 MA in a relatively short period in December 1999. All of the planned plasma shaping parameters, κ = 1.6 – 2.2 and δ = 0.2 – 0.4, were achieved in inner limited, single null and double null configurations. The CHI (Coaxial Helicity Injection) and HHFW (High Harmonic Fast Wave) experiments were also initiated. Using about 27 kA of CHI injected current, discharges of up to 260 kA toroidal current have been produced from zero current without using the ohmic solenoid. Using twelve antennas connected to six transmitters, HHFW successfully heated electrons from central temperature of 400 eV to 900 eV at a central density of 3.5 x 10^{13} cm^{-3} (plasma dielectric constant of 40) with about 2.3 MW of HHFW power. The NBI system commenced operation in Sept. 2000. The initial result with two ion sources (P_{NBI} = 2.8 MW) shows good heating, achieving $\beta_T \approx$ 18 % and a total plasma stored energy of 90 kJ at Ip ≈ 1.1 MA. A summary table for the plasma parameters achieved is shown in Table I.

Heating method	Ohmic	HHFW	NBI
Representative shot	103425	103227	103431
Species	D	He	D
Geometric plasma major radius R_0 (m)	0.86	0.89	0.85
Geometric plasma minor radius a (m)	0.62	0.66	0.62
Plasma current (MA)	0.9	0.7	1.0
Vacuum toroidal field $B_{T0} = B_T(R_0)$ (T)	0.29	0.28	0.30
Magnetic axis major radius R_{axis} (m)	0.96	1.00	0.96
Elongation κ	1.9	1.9	1.9
Triangularity δ	0.34	0.41	0.34
Ohmic power P_{OH} (MW)	1.7	0.9	1.8
Auxiliary power P_{aux} (MW)	–	1.1	2.7
Plasma energy W_{tot} (kJ)	49	51	90
Confinement time τ_E (ms)	30	25	22
Toroidal beta β_T (%)	9	9	17

Normalized beta β_N (%·m·T/MA)	1.9	2.5	3.1
Central electron density n_{e0} ($10^{19}m^{-3}$)	4.1	3.9	3.4
Central electron temperature (keV)	0.3	0.6	0.7

Table 1 Parameters achieved in representative high-β NSTX discharges with different forms of heating. The toroidal beta is defined as $\beta_T = 2\mu_0 <p>/B_{T0}^2$ where <p> is the volume average plasma pressure derived from magnetic data. The normalized beta is defined as $\beta_N = \beta_T \cdot a \cdot B_{T0}/I_p$. The central electron density and temperature are measured by Thomson scattering.

The near-term research program objectives are to bring the NBI and HHFW systems to the full power capability in 2001 (5 MW for NBI and 6 MW for HHFW) and the CHI capability of driving 500 kA of non-inductive start-up current in 2002. With these tools, high beta regimes consistent with the no-wall beta limit of about 25 % (with bootstrap current fraction of up to 40%) will be investigated in the near term (2001-2003). In the longer term (2004 and beyond), more advanced ST regimes will be investigated with active current/pressure profile control (provided by CHI, HHFW, NBI and other tools) and active wall mode stabilization. Development of those plasma control tools is believed to be essential for accessing very advanced ST regimes of steady-state high beta (40%), high bootstrap fraction (70%), and high confinement discharges relevant for the development of an attractive Volume Neutron Source and future power plant.

ACKNOWLEDGEMENTS:

We thank the valuable contributions by the NSTX Technical and Administrative Support Team. The present work is supported by US Dept. of Energy contract No. DE-AC02-76CH03073.

REFERENCES:

[1] M. Y-K. Peng, D.J. Strickler, Nuclear Fusion **26** (1986) 576.
[2] A. SYKES, et al., Plasma Phys. Contr. Nucl. Fus. Res. 1994 **1,** 719 (IAEA,1995).
[3] M. ONO, et al., Plasma Phys. Contr. Nuclear Fusion Research 1996, **2**, 71 (IAEA, 1997).
[4] T. JARBOE, et al., Plasma Phys. Contr. Nuclear Fusion Research 1994, **1**, 725 (IAEA, 1995).
[5] G. REWOLDT, et al., Phys. Plasmas **3**. 1 (1996)
[6] J. MENARD, et al., Nucl. Fusion **37**, 595 (1997).
[7] E.T. CHENG, et al., Fusion Engineering and Design **38**, (1998) 219.
[8] See for example, R. Stambaugh et al., Plasma Phys. Contr. Nuclear Fusion Research 1996, **3**, 395 (IAEA, 1997). F. Najmabadi et al., and D. C. Robinson et al., 17th IAEA Fusion Energy Conference, Yokohama, October 19-24 (1998).
[9] M. ONO, et al., Nucl. Fusion **40**, 557 (2000).
[10] S. KAYE, et al., Fusion Technology, **36**, 16 (1999).
[11] M. ONO, et al., 18th IEEE/NPSS SOFE. 99CH3050, 53 (1999).
[12] M. NAGATA, et al., 17th IAEA Fusion Energy Conference, Yokohama, October 19-24, IAEA-CN-69/EXP4/10 (1998)
[13] M. ONO, Physics of Plasmas **2**, 4075 (1995).
[14] C. NEUMEYER et al. and J. C, J. CHRZANOWSKI, et al., the IEEE SOFE Conference, 99CH3050 (1999).
[15] D. A. GATES, et al., Proc. 11th IEEE Real Time Conference, Santa Fe, USA, 1999, p. 278.
[16] R. MAQUEDA and G. WURDEN, Nucl. Fusion **39** (1999) 629.
[17] S. SABBAGH, et al., IAEA-CN-77/EX3/6, Plasma Phys. Contr. Nuclear Fusion Research 2000 (IAEA, 2001).
[18] J. MENARD, et al., IAEA-CN-77/EXP1/05, Plasma Phys. Contr. Nuclear Fusion Research 2000 (IAEA, 2001).
[19] S. EJIMA, R. CALLIS, J., LUXON, et al., Nucl. Fus. **22** (1982) 1313.
[20] P.YUSHMANOV et al., Nuclear Fusion, **30** (1990)1999.
[21] A. SYKES, et al., IAEA-CN-77/OV4/1, Plasma Phys. Contr. Nuclear Fusion Research 2000 (IAEA, 2001).
[22] R. RAMAN, et al., IAEA-CN-77/EX8/5, Plasma Phys. Contr. Nuclear Fusion Research 2000 (IAEA, 2001).
[23] J. R. WILSON, et al., IAEA-CN-77/EXP1/05, Plasma Phys. Contr. Nuclear Fusion Research 2000 (IAEA, 2001).
[24] D. S. DARROW, et al., in Proceedings of the 26th EPS Conference on Controlled Fusion and Plasma Physics, Maastricht, The Netherlands, 14-18 June 1999, paper P4.090.